First Steps Toward Automatically Generating Bipedal Robotic Walking from Human Data

Aaron D. Ames

Abstract This paper presents the first steps toward automatically generating robotic walking from human walking data through the use of human-inspired control. By considering experimental human walking data, we discover that certain outputs of the human, computed from the kinematics, display the same "universal" behavior; moreover, these outputs can be described by a remarkably simple class of functions, termed *canonical human walking functions*, with a high degree of accuracy. Utilizing these functions, we consider a 2D bipedal robot with knees, and we construct a control law that drives the outputs of the robot to the outputs of the human. Explicit conditions are derived on the parameters of the canonical human walking functions that guarantee that the zero dynamics surface is partially invariant through impact, i.e., conditions that guarantee *partial hybrid zero dynamics*. These conditions therefore can be used as constraints in an optimization problem that minimizes the distance between the human data and the output of the robot. In addition, we demonstrate through simulation that these conditions automatically generate a stable periodic orbit for which the fixed point can be explicitly computed. Therefore, using only human data, we are able to automatically generate a stable walking gait for a bipedal robot which is as "human-like" as possible.

1 Introduction

Obtaining human-like robotic walking has been a long standing, if not always explicitly stated, goal of robotic locomotion. Achieving this goal promises to result in robots able to navigate the myriad of terrains that humans can handle with ease; this would have, for example, important applications to space exploration [4]. Moreover,

A. D. Ames
Department of Mechanical Engineering, Texas A&M University, 3123 TAMU, College Station, TX 77843-3123, e-mail: aames@tamu.edu
This work is supported by NSF grant CNS-0953823 and NHARP award 00512-0184-2009

going beyond purely robotic systems, if one can understand how to make robots walk like humans, this understanding can be used to build robotic assistive and prosthetic devices to aid people with walking impairments and lower extremity amputations walk more efficiently and naturally [29, 8, 22]. Thus, the ability to obtain human-like robotic walking has important and far-reaching ramifications.

The main idea behind this work is that regardless of the complexity present in human walking—hundreds of degrees of freedom coupled with highly nonlinear dynamics and forcing—the essential information needed to understand walking is encoded in simple output functions. That is, we can view the human locomotive system as a "black box" and seek outputs of that system that characterize its behavior in a universally simple fashion or, in other words, attempt to find a low dimensional representation of human walking encoded through outputs described by canonical functions. The goals of this paper are, therefore, two-fold:

1. Determine output functions from human walking data that are accurately described by functions that are canonical, i.e., universal functions of the simplest and most significant form possible.
2. Use these functions to design controllers for a bipedal robot that result in stable walking which is as "close" as possible to human walking.

With the first goal in mind, human data is considered from an experiment where 9 subjects performed straight-line flat-ground walking recorded using motion capture. From the kinematic data associated with this human walking, specific outputs are computed and it is shown that they are accurately described by a very simple class of functions: either a linear function of time, or the time solution to a linear mass-spring-damper system, i.e., a second order linear system response. We therefore achieve the first goal: humans appear to display universally simple behavior when walking, which can be encoded by *canonical human walking functions*. This result provides insight into the basic mechanisms underlying human walking since we conclude that, at the most basic level, the primary outputs associated with locomotion are characterized by a system of linear springs and dampers parameterized in time by the forward walking velocity.

To address the second goal, we consider what we believe to be the simplest bipedal robot that can display "human-like" walking—a 2D robot with knees, modeled as a hybrid system—and we define *human-inspired outputs*: the difference between the outputs of the robot (computed via kinematics) and the human (encoded through canonical walking functions), along with a state-based parameterization of time (achieved through a linear human walking function). Input/output linearization is used to construct an autonomous control law that drives the human-inspired outputs to zero exponentially fast; thus, on the corresponding zero dynamics surface, the outputs of the robot and human are in agreement. We are able to show that, using the human-inspired outputs, we are able to obtain bipedal robotic walking using essentially the same parameters for the human walking functions that were obtained by fitting the data. Yet, due to impacts in the system—which perturb the robot outputs away from the human outputs at foot strike—the resulting walking is reasonably human-like but the velocities are excessively high.

To address the issue of perturbations away from the human outputs at foot strike, we consider the *partial zero dynamics surface* consisting of all of the "relevant" outputs that must be kept invariant through impact, i.e., the relative degree 2 outputs. Conditions are derived—stated only in terms of the parameters of the canonical human walking functions—so that this surface is invariant through impact, i.e., conditions that assure *partial hybrid zero dynamics*. This result is framed as constraints on an optimization problem where the cost function is the sum of residuals squared, resulting in a least squares fit that is as "close" as possible to the human outputs and that ensures invariance of the partial hybrid zero dynamics surface through impact. Even with these constraints, the data for the human outputs is described in a remarkably accurate way by the canonical human walking functions. Moreover, the constraints are constructed in such a way that they automatically produce an initial condition to a stable walking gait for the bipedal robot. We demonstrate this through simulation by obtaining walking for bipedal robots with the mass and length parameters of multiple human subjects. Using only the human walking data, we automatically produce parameters for the human-inspired controller along with a stable walking gait that is as "human-like" as possible.

It is important to note that this is not the first paper that attempts to bridge the gap between human and robotic walking [17, 23, 28, 29], although there have been relatively few studies in this direction when compared to the vast literature on robotic walking and biomechanics (see [9, 10, 11, 33] and[15, 31, 35, 36], to only name a few). Of particular note is [28], which is very much in the same spirit as this paper. In particular, like this paper, that work uses only human parameters and human data to generate human walking, where the least squares fit is used to determine parameters that ensure hybrid zero dynamics. The main difference lies in the output functions and parameterization of time considered. In particular, this paper utilizes canonical human walking functions describing outputs of the human, while [28] considers high degree (9^{th} order) polynomials which are fit directly to the angles of the human over time. This difference is, in the end, a fundamental point of departure. More generally speaking, by looking at outputs of the human that are described by canonical functions intrinsic to walking, the hope is that the fundamental mechanisms underlying human walking can be discovered and exploited to achieve truly human-like bipedal robotic walking.

The structure of this paper is as follows. In Sect. 2 we formally introduce hybrid systems with a view toward modeling bipedal robots. The specific robotic model that will be considered throughout this paper is introduced at the end of the section, where the parameters of the robot are obtained from the humans that performed the walking experiment. This experiment is discussed in Sect. 3, where the canonical human walking functions are introduced, and it is demonstrated that these functions can accurately fit the human output data. Sect. 4 constructs a control law for the bipedal robot based upon the human output functions, and it is shown that this control law can be used to obtain robotic walking—yet the outputs of the robotic walking fail to agree with the human outputs due to the lack of hybrid zero dynamics. In Sect. 5 we remedy this problem through the the formulation of an optimization problem that produces the closest fit of the human walking functions to the human

outputs which guarantee partial hybrid zero dynamics. In Sect. 6, we show through simulation that the parameters solving the optimization problem automatically produce the initial condition to a stable robotic walking gait. This will be demonstrated on robots with parameters from multiple subjects, in addition to an underactuated robot (with no actuation at the ankle) to demonstrate the extensibility of this approach. Finally, conclusions and future directions are discussed in Sect. 7.

2 Lagrangian Hybrid Systems and Robotic Model

Hybrid systems are systems that display both continuous and discrete behavior and so bipedal walkers are naturally modeled by systems of this form, with continuous dynamics when the leg is swinging forward and discrete dynamics when the foot strikes the ground resulting in an instantaneous change in velocity. This section, therefore, introduces the basic terminology of hybrid systems, discusses how to build hybrid models of bipedal robots through hybrid Lagrangians, and applies these constructions to the bipedal robot considered in this paper.

Hybrid Systems. We begin by introducing hybrid (control) systems (also referred to as systems with impulsive effects (or systems with impulse effects [13, 14]); for definitions of hybrid systems that consist of more than one domain, we refer the interested reader to [14, 26]. Note that we can consider hybrid systems with one domain because the biped considered will not have feet; if feet are added to the robot, more complex hybrid systems must be considered. For example, all humans appear to display the same universal discrete structure when walking consisting of four discrete domains [7, 30].

Definition 1. A *hybrid control system* is a tuple,

$$\mathscr{HC} = (X, U, S, \Delta, f, g),$$

where

- X is the *domain* with $X \subseteq R^n$ a smooth submanifold of the state space $\mathbb{R}^n$,
- $U \subseteq \mathbb{R}^m$ is the set of admissible controls,
- $S \subset X$ is a proper subset of X called the *guard* or *switching surface*,
- $\Delta : S \to X$ is a smooth map called the *reset map*,
- (f, g) is a *control system* on X, i.e., in coordinates: $\dot{x} = f(x) + g(x)u$.

A *hybrid system* is a hybrid control system with $U = \emptyset$, e.g., any applicable feedback controllers have been applied, making the system closed-loop. In this case,

$$\mathscr{H} = (X, S, \Delta, f),$$

where f is a *dynamical system* on $X \subseteq \mathbb{R}^n$, i.e., $\dot{x} = f(x)$.

Periodic Orbits. Due to the discrete behavior present in hybrid systems, solutions to these systems (termed executions) are fundamentally different than solutions to dynamical systems. We will forgo the complexity of introducing executions since in the case of bipedal walking we are only interested in periodic solutions. In particular, in the context of bipedal robots, stable walking gaits correspond to stable periodic orbits. With a view towards periodic orbits in the context of bipedal walking, we will introduce periodic orbits of hybrid systems with fixed points on the guard (for more general definitions, see [14, 32]). Let $\varphi(t,x_0)$ be the solution to $\dot{x} = f(x)$ with initial condition $x_0 \in X$. For $x* \in S$, we say that φ is *periodic* with period $T > 0$ if $\varphi(T, \Delta(x*)) = x*$. A set $\mathscr{O}$ is a *periodic orbit* with *fixed point* x^* if $\mathscr{O} = \{\varphi(t,x^*) : 0 \leq t \leq T\}$ for a periodic solution φ. Associated with a periodic orbit is a Poincaré map [32]. In particular, taking S to be the Poincaré section, one obtains the Poincaré map $P : S \to S$ which is a partial function:

$$P(x) = \varphi(T_I(x), \Delta(x)),$$

where T_I is the *time-to-impact function* [33]. As with smooth dynamical systems, the stability of the Poincaré map determines the stability of the periodic orbit $\mathscr{O}$. In particular, the Poincaré map is (locally) exponentially stable (as a discrete time system $x_{k+1} = P(x_k)$) at the fixed point x^* if and only if the periodic orbit $\mathscr{O}$ is (locally) exponentially stable [19]. Although it is not possible to analytically compute the Poincaré map, it is possible to numerically compute its Jacobian. Thus, if the eigenvalues of the Jacobian have magnitude less than one, the stability of the periodic orbit $\mathscr{O}$ has been numerically verified.

Lagrangian Hybrid Systems. Given a bipedal robot, one naturally has a configuration space, a Lagrangian, and a set of admissible constraints (the swing foot must remain above the ground). This information, inherent to a specific robot, can be encoded formally as a hybrid Lagrangian [5]:

Definition 2. A *hybrid Lagrangian* is a tuple:

$$\mathscr{L} = (Q, L, h),$$

where

- Q is the configuration space,
- $L : TQ \to \mathbb{R}$ is a hyperregular Lagrangian,
- $h : Q \to \mathbb{R}$ provides unilateral constraints on the configuration space; it is assumed that $h^{-1}(0)$ is a manifold.

Using a hybrid Lagrangian, we can explicitly construct a hybrid system.

Continuous Dynamics: The Lagrangian of a bipedal robot, $L : TQ \to \mathbb{R}$, can be stated in the form of the kinetic minus potential energy as:

$$L(q,\dot{q}) = \frac{1}{2}\dot{q}^T D(q)\dot{q} - V(q).$$

The Euler-Lagrange equations yield the equations of motion; for robotic systems (see [20]), these are of the form:

$$D(q)\ddot{q}+H(q,\dot{q})=B(q)u.$$

Converting the equations of motion to a first order ODE yields the affine control system (f,g):

$$f(q,\dot{q})=\begin{bmatrix}\dot{q}\\ -D^{-1}(q)H(q,\dot{q})\end{bmatrix},\qquad g(q)=\begin{bmatrix}\mathbf{0}\\ D^{-1}(q)B(q)\end{bmatrix}. \tag{1}$$

Domain and Guard: The domain specifies the allowable configuration of the system as specified by the unilateral constraint function h; for the biped considered in this paper, this function specifies that the non-stance foot must be above the ground. In particular, the domain X is given by:

$$X=\{(q,\dot{q})\in TQ : h(q)\geq 0\}. \tag{2}$$

The guard is just the boundary of the domain with the additional assumption that the unilateral constraint is decreasing:

$$S=\{(q,\dot{q})\in TQ : h(q)=0 \text{ and } dh(q)\dot{q}<0\}, \tag{3}$$

where $dh(q)$ is the Jacobian of h at q.

Discrete Dynamics: In order to define the reset map, it is necessary to first augment the configuration space Q. Let p represent the Cartesian position of the stance foot in the x,z plane. The *generalized coordinates* are then written as $q_e=(p_x,p_z,q)\in Q_e=\mathbb{R}^2\times Q$. Without loss of generality, assume that the values of the extended coordinates are zero throughout the gait, i.e., the stance foot will be fixed at the origin. Therefore, consider the embedding $\iota : Q\to Q_e$ defined as $q\mapsto(0,0,q)$; associated with this embedding is a canonical projection $\pi : Q_e\to Q$.

We employ the impact model described in [16]; that is, plastic rigid-body impacts with impulsive forces are used to simulate impact. In particular, impulsive forces are applied to the swing foot when it contacts the ground. Let $\Upsilon(q_e)$ be the x,z position of the end of the non-stance leg relative to the x,z position of the stance leg $(p_x,\ p_z)$ and let $J(q_e)=d\Upsilon(q_e)$ be the Jacobian of Υ. The *impact map* gives the post-impact velocity:

$$\dot{q}_e^+=\mathscr{P}_e(q_e)\dot{q}_e^-=(I-D^{-1}(q_e)J^T(q_e)(J(q_e)D^{-1}(q_e)J^T(q_e))^{-1}J(q_e))\dot{q}_e^- \tag{4}$$

with I the identity matrix.

In the bipedal walking literature, under the assumption of symmetric walking, it is common to use a stance/non-stance notation for the legs [13] rather than considering the left and right leg separately; it is more intuitive to think of control design for the legs in the context of stance/non-stance than left/right. To achieve this, the legs must be "swapped" at impact. A coordinate transformation $\mathscr{R}$ (*state relabeling*

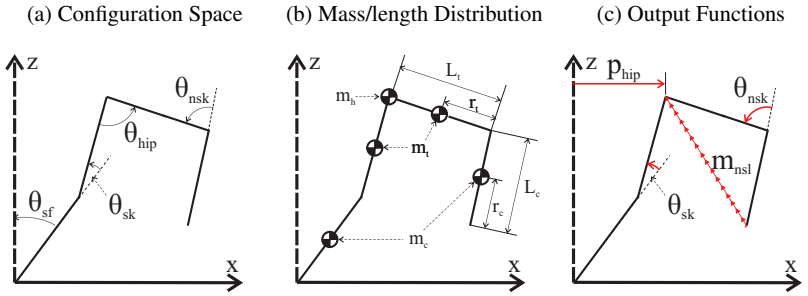

Fig. 1: Configuration variables (a) and mass/length distribution (b) of the bipedal robot, along with the output functions of the robot considered (c).

procedure) switches the roles of the left and right legs and is included in the reset map:

$$\Delta : S \to X, \qquad \Delta(q,\dot{q}) = \begin{bmatrix} \mathscr{R} & \mathbf{0} \\ \mathbf{0} & \mathscr{R} \end{bmatrix} \begin{bmatrix} q \\ \mathscr{P}(q)\dot{q} \end{bmatrix}, \tag{5}$$

where

$$\mathscr{P}(q) = d\pi(\iota(q))\mathscr{P}_e(\iota(q))d\iota(q)$$

with $d\pi$ the Jacobian of the projection π and $d\iota$ the Jacobian of the embedding ι.

Bipedal Robot Model. In this paper, we consider a 2-dimensional bipedal robot with knees as illustrated in Fig. 1. The motivation for considering this specific model is that it is simple enough to make the discussion of ideas related to human-inspired control more concise, while being complex enough to display interesting behavior. Using the previous constructions of this section, we explicitly construct a hybrid model.

Hybrid Lagrangian: The 2D kneed biped with knees has four links, yielding a configuration space Q_R with coordinates: $\theta = (\theta_{sf}, \theta_{sk}, \theta_{hip}, \theta_{nsk})^T$, where, as illustrated in Fig. 1(a), θ_{sf} is the angle of the stance foot, θ_{sk} is the angle of the stance knee, θ_{hip} is the angle of the hip and θ_{nsk} is the angle of the non-stance (or swing) knee. Combining this choice of coordinates with the mass and length distribution illustrated in Fig. 1(b) (with parameters chosen from the table in Fig. 2(b)) yields a Lagrangian L_R which depends on the parameters (lengths and masses) of the specific human subject being considered (as discussed in Sect. 3). Finally, the unilateral constraint is simply the height of the non-stance foot above the ground: h_R (which again depends on the parameters of the specific subject being considered). The end result is that, given a bipedal robot model with parameters obtained from a specific subject, we obtain a hybrid Lagrangian:

$$\mathscr{L}_R = (Q_R, L_R, h_R). \tag{6}$$

Hybrid System Model: From this hybrid Lagrangian we obtain a hybrid system model for the robot with the parameters from a specific subject:

$$\mathscr{HC}_R = (X_R, U_R, S_R, \Delta_R, f_R, g_R), \tag{7}$$

where here the domain and guard, X_R and S_R, are given by (2) and (3), respectively, using the unilateral constraint function h_R, $U_R = \mathbb{R}^4$ since we do not put any restrictions on the set of admissible controls and assume full actuation, and Δ_R is given by (5) with relabeling matrix:

$$\mathscr{R} = \begin{bmatrix} 1 & 1 & -1 & -1 \\ 0 & 0 & 0 & 1 \\ 0 & 0 & -1 & 0 \\ 0 & 1 & 0 & 0 \end{bmatrix}, \tag{8}$$

which switches the stance and non-stance leg at impact. Note that we assume full actuation because during the course of a human step, most of the time is spent in domains where there is full actuation [7]. Moreover, methods for extending control laws assuming full actuation to domains with underactuation have been discussed in [14, 25, 26]. Also note that the methods discussed in this section can be used to "automatically" generate a wide variety of bipedal robotic models (see [24] for 3 other single-domain models and [7] for the multi-domain case). Finally, to further justify this point, we consider the case of underactuation at the end of Sect. 6 and show that we can also obtain walking when the stance ankle, θ_{sf}, is not actuated.

3 Canonical Human Walking Functions

This section begins by discussing a human walking experiment. We use the data from this experiment to motivate the introduction of canonical human walking functions. Amazingly, these functions are very simple; they describe the solution to a linear spring-damper system. The use of these functions is justified by fitting them to certain outputs of the human computed from the experimental data, resulting in very high correlation fits. We conclude, therefore, that humans display very simple behavior when the proper outputs are considered.

Human Walking Experiment. Data was collected on 9 subjects using the Phase Space System, which computes the 3D position of 19 LED sensors at 480 frames per second using 12 cameras at 1 millimeter level of accuracy. The cameras were calibrated prior to the experiment and were placed to achieve a 1 millimeter level of accuracy for a space of size 5 by 5 by 5 meters cubed. Six sensors were placed on each leg at the joints; a sensor was placed on each leg at the heel and another at the toe; finally, one sensor was placed at each of the following locations: the sternum, the back behind the sternum and the belly button (as illustrated in Fig. 2). Each trial of the experiment required the subject to walk 3 meters along a line drawn on

(a) Experimental Setup

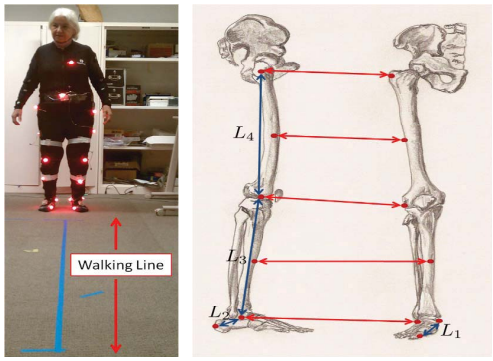

(b) Subject Parameters

Subject	S_1	S_2	S_3
Sex	M	M	F
Age	22	30	23
Ht. (cm)	169.5	170.0	165.5
Wt. (kg)	90.9	69.1	47.7
m_h (kg)	61.5	46.7	32.3
m_t (kg)	9.1	6.9	4.8
m_c (kg)	5.5	3.3	2.9
L_t (cm)	40.1	43.8	39.2
L_c (cm)	43.5	38.1	37.6

Fig. 2: (a) Illustrations of the experimental setup and sensor placement. Each LED sensor was placed at the joints as illustrated with the dots on the right lateral and anterior aspects of each leg. (b) The physical parameters of the 3 subjects considered in this paper, together with the mapping of those parameters onto the robot being considered (see Fig. 1(b)).

the floor. Each subject performed 12 trials, which constituted a single experiment. 3 female and 6 male subjects with ages ranging between 17 and 77 years, heights ranging between 161 and 189 centimeters, and weights ranging between 47.6 and 90.7 kilograms. The data for each individual is rotated so that the walking occurs in the x-direction, and for each subject the 12 walking trials are averaged (after appropriately shifting the data in time). The collected data is available at [2].

In this paper, for the sake of simplicity of exposition, we will consider the data for 3 of these 9 subjects. The parameters for these 3 subjects as they are used on the bipedal robot can be found in the table in Fig. 2(b). To map the human parameters that were experimentally determined to the robotic model being considered, the standard mass distribution formula from [35] was used.

Human Outputs and Walking Functions. The fundamental idea behind obtaining robotic walking from human walking data is that, rather than looking at the dynamics of the human, one should look at outputs of the human that represent the walking behavior. By tracking these outputs in a robot, through their representation via canonical functions, the robot will display the same qualitative behavior as the human despite the differences in dynamics. That is, we seek to find a "low-dimensional" representation of human walking. To find this representation, we look for "simple" functions of the kinematics of the human that seem to be representative of walking, termed *canonical human walking functions*.

The specific choice of human outputs to consider depend on the bipedal robot. In particular, and roughly speaking, for each degree of freedom of the robot there must be an associated output. In addition, these outputs must not "compete" with each

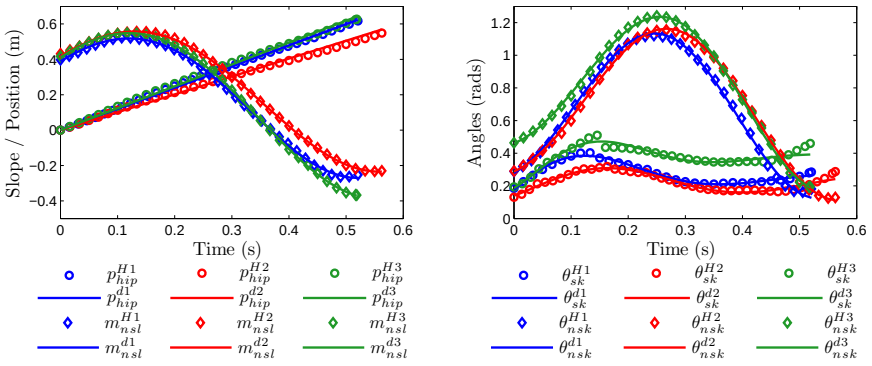

(a) Hip Position and Non-Stance Leg Slope (b) Stance and Non-stance Knee Angle, θ_{nsk}

Fig. 3: The human output data and the canonical walking function fits for each subject.

other, i.e., they must be mutually exclusive; formally speaking, this means that the decoupling matrix associated with these outputs must be non-singular (as will be discussed in Sect. 6). Motivated by intuition, and after the consideration of a large number of human outputs, the four we have found to be most essential to walking in the case of the robot being considered are:

1. The x-position of the hip, p_{hip},
2. The slope of the non-stance leg, i.e., the tangent of the angle between the z-axis and the line on the non-stance leg connecting the ankle and hip:

$$m_{nsl} = \frac{p^x_{nsf} - p_{\text{hip}}}{p^z_{nsf} - p^z_{\text{hip}}},$$

   where p^z_{hip} is the z-position of the hip and p^x_{nsf}, p^z_{nsf} are the x and z position of the non-stance foot, respectively,
3. The angle of the stance knee, θ_{sk},
4. The angle of the non-stance knee, θ_{nsk} .

These outputs can be seen in Fig. 1(c).

Visually inspecting the outputs as computed from the human data for the three subjects, as shown in Fig. 3, all of the human outputs appear to be described by two simple functions:

$$\begin{aligned} p_{\text{hip}}: &\qquad y_{H,1}(t,v) = vt, \\ m_{nsl},\, \theta_{sk},\, \theta_{nsk}: &\qquad y_{H,2}(t,\alpha) = e^{-\alpha_4 t}(\alpha_1 \cos(\alpha_2 t) + \alpha_3 \sin(\alpha_2 t)) + \alpha_5, \end{aligned} \tag{9}$$

where $\alpha = (\alpha_1, \alpha_2, \alpha_3, \alpha_4, \alpha_5)$. Moreover, these functions appear to be *universal* to walking, in that all of the subjects considered in this experiment followed functions

of this form for the chosen outputs. Of special interest is the fact that $y_{H,1}$ simply parameterizes time by the forward velocity (walking speed) of the human and $y_{H,2}$ is simply the solution to a linear mass-spring-damper system with constant external forcing [12]. Thus, despite the complexity of the internal dynamics inherent to walking, humans appear to act like a linear spring damper system parameterized by the walking speed.

It is important to note that this universality continues beyond the robotic model considered in this paper. In fact, we have found that this pattern continues for robots with feet [25] and for 3-dimensional robots [24], i.e., the additional human outputs that must be considered for these robots due to the additional degrees of freedom can be described by $y_{H,2}$ with a high degree of accuracy (a high correlation coefficient).

Data-Based Cost Function. Having obtained what we believe to be outputs characterized by functions that appear to be canonical to human walking, it is necessary to determine the specific parameters of these functions that best fit the human data. While this can be done with a myriad of software programs, we describe the procedure to fit these functions in terms of minimizing a cost function; the reason for explicitly stating the cost function is that this same cost function is used when considering hybrid zero dynamics, except that it is subject to constraints.

As a result of the universality of the human walking functions (9), we can consider these functions for each of the subjects and each of the outputs specified above: p_{hip}, m_{nsl}, θ_{sk}, and θ_{nsk}. This yields the following four functions that we wish to fit to the data for each subject:

$$\begin{aligned} p^d_{\text{hip}}(t, v_{\text{hip}}) &= y_{H,1}(t, v_{\text{hip}}), & m^d_{nsl}(t, \alpha_{nsl}) &= y_{H,2}(t, \alpha_{nsl}), \\ \theta^d_{sk}(t, \alpha_{sk}) &= y_{H,2}(t, \alpha_{sk}), & \theta^d_{nsk}(t, \alpha_{nsk}) &= y_{H,2}(t, \alpha_{nsk}), \end{aligned} \tag{10}$$

where, for example, $\alpha_{nsl} = (\alpha_{nsl,1}, \alpha_{nsl,2}, \alpha_{nsl,3}, \alpha_{nsl,4}, \alpha_{nsl,5})$ in (9). The parameters for the four output functions can be combined to yield a single vector of parameters: $\alpha = (v_{\text{hip}}, \alpha_{nsl}, \alpha_{nsk}, \alpha_{sk}) \in \mathbb{R}^{16}$ for each subject. These output functions can be directly compared to the corresponding human data. In particular, from the human walking experiment, we obtain discrete times, $t^H[k]$, and discrete values for the output functions: $p^H_{\text{hip}}[k]$, $m^H_{nsl}[k]$, $\theta^H_{sk}[k]$ and $\theta^H_{nsk}[k]$, for $k \in \{1, \dots, K\} \subset \mathbb{N}$ with K the number of data points.

Consider the following human-data-based cost function:

$$\begin{aligned} &\text{Cost}_{\text{HD}}(\alpha) = \\ &\sum_{k=1}^{K} \Big(\beta_{p_{\text{hip}}} (p^d_{\text{hip}}(t^H[k], v_{\text{hip}}) - p^H_{\text{hip}}[k])^2 + \beta_{m_{nsl}} (m^d_{nsl}(t^H[k], \alpha_{nsl}) - m^H_{nsl}[k])^2 \\ &\qquad + \beta_{\theta_{sk}} (\theta^d_{sk}(t^H[k], \alpha_{sk}) - \theta^H_{sk}[k])^2 + \beta_{\theta_{nsk}} (\theta^d_{nsk}(t^H[k], \alpha_{nsk}) - \theta^H_{nsk}[k])^2 \Big), \end{aligned} \tag{11}$$

where each of the weightings, β, are the reciprocal of the difference of the maximum and minimum value of the human data for that output. Therefore, this cost function is simply the weighted sum of the squared residuals. Clearly, this cost function de-

Table 1: Table containing parameter values of the canonical human walking functions for the 3 subjects together with the cost and correlations of the fits.

$y_{H,1} = vt$ $y_{H,2} = e^{-\alpha_4 t}(\alpha_1 \cos(\alpha_2 t) + \alpha_3 \sin(\alpha_2 t)) + \alpha_5$									
S	Fun.	v	α_1	α_2	α_3	α_4	α_5	Cost	Cor.
1	p_{hip}	1.1969	*	*	*	*	*	0.017	0.9995
	m_{nsl}	*	0.2021	7.8404	0.2248	-0.8070	0.1871		0.9998
	θ_{sk}	*	-0.0828	13.316	0.2073	4.1551	0.2574		0.9933
	θ_{nsk}	*	-0.3809	-10.979	-0.1966	-0.4215	0.6585		0.9990
2	p_{hip}	1.0104	*	*	*	*	*	0.029	0.9992
	m_{nsl}	*	0.2040	7.3406	0.2417	-0.6368	0.2147		0.9999
	θ_{sk}	*	-0.0800	13.379	0.0865	1.6614	0.2198		0.9807
	θ_{nsk}	*	-0.3914	-10.516	-0.1562	-0.5243	0.6789		0.9995
3	p_{hip}	1.2372	*	*	*	*	*	0.057	0.9990
	m_{nsl}	*	0.2618	7.2804	0.2615	-0.6769	0.1490		1.0000
	θ_{sk}	*	-0.1939	16.152	0.0745	4.9945	0.3801		0.9561
	θ_{nsk}	*	-0.3190	10.903	0.1539	-1.0190	0.7790		0.9995

pends on the output data for a specific subject over the course of one step, together with the choice of walking functions (10), but it is viewed only as a function of the vector of parameters $\alpha = (v_{\text{hip}}, \alpha_{nsl}, \alpha_{sk}, \alpha_{nsk})$. To determine this vector of parameters, we need only solve the following optimization problem:

$$\alpha^* = \underset{\alpha \in \mathbb{R}^{16}}{\text{argmin}} \ \text{Cost}_{\text{HD}}(\alpha) \tag{12}$$

which yields the least squares fit of the data with the canonical walking functions; again, the reason for restating this standard definition is that this same cost function will be used in Sect. 5, but subject to specific constraints that ensure hybrid zero dynamics. The parameters given by solving this optimization problem are stated in Table 1 along with the cost (11) associated with these parameters. The correlations, as given in the same table, show that the fitted walking functions very closely model the human output data, i.e., the chosen human walking functions appear to be, in fact, canonical. Indeed, the coefficients of correlation are all between 0.9561 and 1.000. The accuracy of the fits can be seen in Fig. 3.

4 Human-Inspired Control

In this section, we construct a human-inspired controller that drives the outputs of the robot to the outputs of the human (as represented by canonical walking functions). Moreover, we are able to make this control law autonomous through a parameterization of time based upon the position of the hip. The end result is a feedback control that yields stable walking when applied to the bipedal robot being

considered. The aspects of this walking are discussed—specifically, the fact that the outputs are not left invariant through impact—in order to motivate the introduction of hybrid zero dynamics in the next section.

Output Functions. Based upon the canonical human walking functions, we define the following relative degree one and two outputs for the bipedal robot being considered (see Sect. 2 for the robot and [21] for the definition of relative degree):

Relative Degree 1: Recall that the forward position of the hip of the human is described by: $p^d_{\text{hip}}(t, v_{\text{hip}}) = v_{\text{hip}} t$. Therefore, the forward velocity of a human when walking is approximately constant, and we wish to define an output that will similarly keep the forward velocity of the robot constant. Letting $p^R_{\text{hip}}(\theta)$ be the x-position of the robot (which is computed through forward kinematics), the goal is to drive: $\dot{p}^R_{\text{hip}} \to v_{\text{hip}}$. With this in mind, we define the following actual and desired outputs:

$$y_{a,1}(\theta, \dot{\theta}) = d p^R_{\text{hip}}(\theta)\dot{\theta}, \qquad y_{d,1} = v_{\text{hip}}. \tag{13}$$

Note that $y_{a,1}$ will be a relative degree 1 output since it is the output of a mechanical system depending both on position and velocity.

Relative Degree 2: We now consider the remainder of the outputs given in (10); in particular, we consider the non-stance leg slope, m_{nsl}, the stance knee angle, θ_{sk} and the non-stance knee angle, θ_{nsk}. The stance slope of the robot can be stated in terms of the angles of the system through the use of kinematics, i.e., we obtain an expression $m^R_{nsl}(\theta)$. Since the goal is for the robot to track the human outputs, we consider the following actual and desired outputs:

$$y_{a,2}(\theta) = \begin{bmatrix} m^R_{nsl}(\theta) \\ \theta_{sk} \\ \theta_{nsk} \end{bmatrix}, \qquad y_{d,2}(t) = \begin{bmatrix} m^d_{nsl}(t, \alpha_{nsl}) \\ \theta^d_{sk}(t, \alpha_{sk}) \\ \theta^d_{nsk}(t, \alpha_{nsk}) \end{bmatrix}. \tag{14}$$

Since the actual output is only a function of the configuration variables for a mechanical system, it will be relative degree 2.

Parameterization of Time. The goal is clearly to drive $y_{a,1} \to y_{d,1}$ and $y_{a,2} \to y_{d,2}$. This could be done through standard tracking control laws [21], but the end result would be a time-based, or non-autonomous, control law. This motivates the introduction of a parameterization of time in order to obtain an autonomous control law. This procedure is common in the literature [33, 34], and the parameterization chosen draws inspiration from both those that have been used in the past in the context of bipedal walking and the human data. Using the fact that the forward position of the hip of the human is described by $p^d_{\text{hip}}(t, v_{\text{hip}}) = v_{\text{hip}} t$, for the human: $t \approx \frac{p_{\text{hip}}}{v_{\text{hip}}}$. This motivates the following parameterization of time for the robot:

$$\tau(\theta) = \frac{p^R_{\text{hip}}(\theta) - p^R_{\text{hip}}(\theta^+)}{v_{\text{hip}}}, \tag{15}$$

where here $p^R_{\text{hip}}(\theta^+)$ is the position of the hip of the robot at the beginning of a step[1] with θ^+ assumed to be a point where the height of the non-stance foot is zero, i.e., $h_R(\theta^+) = 0$, with h_R the unilateral constraint for the hybrid Lagrangian $\mathscr{L}_R$ associated with the bipedal robot (6).

Control Law Construction. Using the parameterization of time, we define the following output functions, termed *human-inspired outputs*:

$$\begin{aligned} y_1(\theta,\dot\theta) &= y_{a,1}(\theta,\dot\theta) - y_{d,1},\\ y_2(\theta) &= y_{a,2}(\theta) - y_{d,2}(\tau(\theta)), \end{aligned} \tag{16}$$

which depend on the specific choice of parameters, α, for the human walking functions, where y_1 is an output with relative degree 1 and y_2 is a vector of outputs all with relative degree 2. For the affine control system (f_R, g_R) associated with the robotic model being considered (7), we define the following control law:

$$u(\theta,\dot\theta) = -A^{-1}(\theta,\dot\theta)\left(\begin{bmatrix} 0 \\ L^2_{f_R} y_2(\theta,\dot\theta)\end{bmatrix} + \begin{bmatrix} L_{f_R} y_1(\theta,\dot\theta) \\ 2\varepsilon L_{f_R} y_2(\theta,\dot\theta)\end{bmatrix} + \begin{bmatrix} 2\varepsilon y_1(\theta,\dot\theta) \\ \varepsilon^2 y_2(\theta)\end{bmatrix}\right), \tag{17}$$

with L the Lie derivative and A the decoupling matrix:

$$A(\theta,\dot\theta) = \begin{bmatrix} L_{g_R} y_1(\theta,\dot\theta) \\ L_{g_R} L_{f_R} y_2(\theta,\dot\theta)\end{bmatrix}. \tag{18}$$

Note that the decoupling matrix is non-singular exactly because of the choice of output functions, i.e., as was discussed in Sect. 3, care was taken when defining the human outputs so that they were "mutually exclusive." It follows that for a control gain $\varepsilon > 0$, the control law u renders the output exponentially stable [21]. That is, the human-inspired outputs $y_1 \to 0$ and $y_2 \to 0$ exponentially at a rate of ε; in other words, the outputs of the robot will converge to the canonical human walking functions exponentially. In addition, since $y_1 \to 0$, it follows that during the continuous evolution of the system $y_{a,1} = \dot p^R_{\text{hip}} \to v_{\text{hip}}$, i.e., the velocity of the hip will converge to the velocity of the human, thus justifying the parameterization of time given in (15).

Applying the feedback control law in (17) to the hybrid control system modeling the bipedal robot being considered, $\mathscr{HC}_R$ as given in (7), yields a hybrid system:

$$\mathscr{H}^{(\alpha,\varepsilon)}_R = (X_R, S_R, \Delta_R, f^{(\alpha,\varepsilon)}_R), \tag{19}$$

where, X_R, S_R, and Δ_R are defined as for $\mathscr{HC}_R$, and

$$f^{(\alpha,\varepsilon)}_R(\theta,\dot\theta) = f_R(\theta,\dot\theta) + g_R(\theta,\dot\theta)u(\theta,\dot\theta),$$

[1] Note that we can assume that the initial position of the human is zero, while this cannot be assumed for the robot since the initial position of the hip will depend on the specific choice of configuration variables for the robot.

where the dependence of $f_R^{(\alpha,\varepsilon)}$ on the vector of parameters, α, and the control gain for the input/output linearization control law, ε, has been made explicit.

Partial Hybrid Zero Dynamics. In addition to driving the chosen outputs to zero, i.e., driving the outputs of the robot to the outputs of the human, the control law (17) also renders the *(full) zero dynamics surface*:

$$\mathbf{Z}_\alpha = \{(\theta,\dot{\theta}) \in TQ : y_1(\theta,\dot{\theta}) = 0,\ y_2(\theta) = \mathbf{0},\ L_{f_R} y_2(\theta,\dot{\theta}) = \mathbf{0}\} \tag{20}$$

invariant for the continuous dynamics; here, $\mathbf{0} \in \mathbb{R}^3$ is a vector of zeros and we make the dependence of $\mathbf{Z}_\alpha$ on the set of parameters explicit. This fact is very important for continuous control systems since once the outputs converge to zero, they will stay at zero. The difficulty of ensuring these conditions in the case of hybrid systems will be discussed in Sec. 5. In particular, in the case of the robot considered in this paper, we will seek only to enforce the zero dynamics surface related to the relative degree 2 outputs. We refer to this as the *partial zero dynamics surface*, given by:

$$\mathbf{PZ}_\alpha = \{(\theta,\dot{\theta}) \in TQ : y_2(\theta) = \mathbf{0},\ L_{f_R} y_2(\theta,\dot{\theta}) = \mathbf{0}\} \tag{21}$$

The motivation for considering this surface is that it allows some "freedom" in the movement of the system to account for differences between the robot and human models. Moreover, since the only output that is not included in the partial zero dynamics surface is the output that forces the forward hip velocity to be constant, enforcing partial hybrid zero dynamics simply means that we allow the velocity of the hip to compensate for the shocks in the system due to impact.

As a final note, the partial zero dynamics surface is simply the zero dynamics surface considered in [33]; that is, in that reference and all of the supporting papers, underactuation at the stance ankle is considered (this case will be addressed, in the context of human-inspired control, in Sect. 6). It is exactly the stance ankle that we control via the output y_1. Thus, in essence, the partial zero dynamics is just the classical zero dynamics surface considered in the bipedal walking literature. Therefore, if parameters can be determined that render this surface invariant through impact, the system will evolve on a 2-dimensional zero dynamics manifold. The main differences separating this work from existing work is that the shape of the zero dynamics surface—as determined by the human outputs and the parameters of the human walking function—is chosen explicitly from human data.

Robotic Walking without Hybrid Zero Dynamics. To demonstrate that it is possible to obtain human walking with the human-inspired outputs, we manually looked for periodic orbits for the hybrid system $\mathscr{H}_R^{(\alpha,\varepsilon)}$, with α a vector of parameters as "close" as possible to the vector of parameters α^* solving the optimization problem (12). In particular, we considered Subject 1 and his corresponding mass and length parameters (Fig. 2(b)). We found that by only changing α_5 for m_{nsl} in Table 1 from 0.1871 to 0.0623, and picking $\varepsilon = 20$, we were able to obtain a stable periodic orbit, i.e., a stable walking gait, as seen in Fig. 4. The stability of the periodic orbit was checked by numerically computing the eigenvalues of the Poincaré map; the mag-

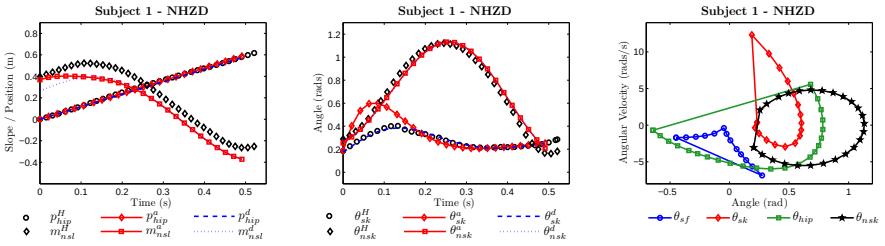

(a) p_{hip} and m_{nsl} (b) θ_{sk} and θ_{nsk} (c) Periodic Orbit

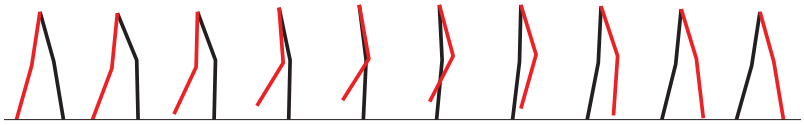

(d) Walking Tiles

Fig. 4: Walking obtained for Subject 1 without hybrid zero dynamics, with (a)-(b) the actual and desired outputs vs. the human output data over one step, (c) the periodic orbit and (d) the tiles (or snapshots) of the walking gait.

nitude of these eigenvalues and the corresponding fixed point can be found in Fig. 7. Finally, a movie of the walking can be found at [1].

The robotic walking shown in Fig. 4 allows one to draw some important conclusions. Despite the fact that the parameters α used to obtain the walking are almost identical to the parameters obtained by fitting the canonical output functions to the human data, as seen in Figs. 4(a)-(b), the outputs of the robot are dramatically different than those seen in the human data. This is a direct result of the fact that the zero dynamics surface $\mathbf{Z}_\alpha$ is not invariant through impact, i.e., there are not hybrid zero dynamics. Therefore, at impact, the robot is thrown off the zero dynamics surface, resulting in the parameterization of time, τ, becoming highly nonlinear. Since the other desired functions depend on this parameterization, this changes the shape of these functions in a nonlinear fashion and thus the shape of the zero dynamics surface. Moreover, the fact that the control law tries to drive the outputs to zero means that after impact a spike in both velocity and torque occurs (the angular velocity after impact exceeds $12\frac{rad}{s}$ as seen in Fig. 4(c)). The end result is that while this control yields stable walking, it is unrealistic in a physical context. In order to solve this issue, it is clearly necessary to determine conditions that guarantee that the zero dynamics are invariant through impact.

5 Partial Hybrid Zero Dynamics for Human-Inspired Outputs

The goal of this section is to find parameters that result in *partial hybrid zero dynamics* (PHZD) while best fitting the human walking data. The main result is that we are able to formulate an optimization problem, *only* depending on the parameters α, that guarantees PHZD. We demonstrate this optimization problem on the human subject data, showing that we are able to simultaneously achieve PHZD and very good fits of the human data with the canonical human walking functions.

Problem Statement: PHZD. The goal of human-inspired PHZD is to find parameters α^* that solve the following constrained optimization problem:

$$\alpha^* = \underset{\alpha \in \mathbb{R}^{16}}{\operatorname{argmin}} \ \text{Cost}_{\text{HD}}(\alpha) \tag{22}$$

$$\text{s.t} \quad \Delta_R(S_R \cap \mathbf{Z}_\alpha) \subset \mathbf{PZ}_\alpha \tag{PHZD}$$

with Cost_{HD} the cost given in (11), $\mathbf{Z}_\alpha$ the full zero dynamics surface given in (20) and $\mathbf{PZ}_\alpha$ the partial zero dynamics surface given in (21). This is simply the optimization problem in (12) that was used to determine the parameters of the canonical human walking functions that gave the best fit of the human output data, but subject to constraints that ensure PHZD.

The formal goal of this section is to restate (PHZD) in such a way that it can be practically solved; as (22) is currently stated, it depends on both the parameters, α, as well as the state of the robot, $(\theta, \dot{\theta})$, due to the inclusion of the (full and partial) zero dynamics surfaces $\mathbf{Z}_\alpha$ and $\mathbf{PZ}_\alpha$ in the constraints.

Position and Velocity from Parameters. To acheive the goal of restating (22) in a way that is independent of state variables (position and velocity), we can use the outputs and guard functions to explicitly solve for the configuration of the system $\vartheta(\alpha) \in Q_R$ on the guard in terms of the parameters. In particular, let

$$\vartheta(\alpha) = \theta \quad \text{s.t} \quad \begin{bmatrix} y_2(\mathscr{R}\theta) \\ h_R(\theta) \end{bmatrix} = \begin{bmatrix} \mathbf{0} \\ 0 \end{bmatrix}, \tag{23}$$

where $\mathscr{R}$ is the relabeling matrix (8). Note that $\vartheta(\alpha)$ exists because of the specific structure of the outputs, $y_2(\mathscr{R}\theta)$, chosen. In fact, the reason for considering y_2 at the point $\mathscr{R}\theta$ is because this implies that the configuration at the beginning of the step is $\theta^+ = \mathscr{R}\theta$ and thus $\tau(\mathscr{R}\theta) = 0$ implying that:

$$y_2(\mathscr{R}\theta) = y_{a,2}(\mathscr{R}\theta) - y_{d,2}(0),$$

or there is a solution to (23) because of the simple form that y_2 takes at the point $\mathscr{R}\theta$. Also note that since solving for $\vartheta(\alpha)$ is essentially an inverse kinematics problem, the solution obtained exists, but is not necessarily unique. Therefore, a solution must be picked that is "reasonable," i.e., θ_{sf} and θ_{hip} are in $[-\frac{\pi}{2}, 0]$, and that produces the first time when the foot hits the ground, $\tau(\vartheta(\alpha))$.

Using $\vartheta(\alpha)$, we can explicitly solve for velocities $\dot{\vartheta}(\alpha)$. The methodology is to solve for the velocities that are in the full zero dynamics surface $\mathbf{Z}_\alpha \subset \mathbf{PZ}_\alpha$ pre-impact as motivated by the fact that solutions will converge to this surface exponentially during the walking gait; thus, the velocities pre-impact will be sufficiently close to this point even if we only enforce partial hybrid zero dynamics. In particular, let

$$Y(\theta) = \begin{bmatrix} dp^R_{\text{hip}}(\theta) \\ dy_2(\theta) \end{bmatrix}, \tag{24}$$

with $dp_{\text{hip}}(\theta)$ and $dy_2(\theta)$ the Jacobian of p_{hip} and y_2, respectively. It follows from (13), (14), (16), and the fact that y_2 is a relative degree 2 output that

$$\begin{bmatrix} y_1(\theta,\dot{\theta}) \\ L_{f_R} y_2(\theta,\dot{\theta}) \end{bmatrix} = Y(\theta)\dot{\theta} - \begin{bmatrix} v_{\text{hip}} \\ \mathbf{0} \end{bmatrix}. \tag{25}$$

Therefore, define

$$\dot{\vartheta}(\alpha) = Y^{-1}(\vartheta(\alpha)) \begin{bmatrix} v_{\text{hip}} \\ \mathbf{0} \end{bmatrix}. \tag{26}$$

Note that Y is invertible, again because of the specific choice of outputs, i.e., because of the relative degree of the outputs y_1 and y_2.

PHZD Optimization. We now present the first main result of this paper. Using $\vartheta(\alpha)$ and $\dot{\vartheta}(\alpha)$, we can restate the optimization problem (22) in terms of only parameters of the system. Moreover, as will be seen Sect. 6, by solving the restated optimization problem, we automatically obtain an initial condition corresponding to stable periodic walking.

Theorem 1. *The parameters α^* solving the constrained optimization problem:*

$$\begin{aligned} \alpha^* = \underset{\alpha\in\mathbb{R}^{16}}{\text{argmin}}\ & \text{Cost}_{\text{HD}}(\alpha) && (27)\\ \text{s.t}\quad & y_2(\vartheta(\alpha)) = \mathbf{0} && \text{(C1)}\\ & dy_2(\mathscr{R}\vartheta(\alpha))\mathscr{R}\mathscr{P}(\mathscr{R}\vartheta(\alpha))\dot{\vartheta}(\alpha) = \mathbf{0} && \text{(C2)}\\ & dh_R(\vartheta(\alpha))\dot{\vartheta}(\alpha) < 0 && \text{(C3)} \end{aligned}$$

yield partial hybrid zero dynamics: $\Delta_R(S_R \cap \mathbf{Z}_{\alpha^*}) \subset \mathbf{PZ}_{\alpha^*}$.

Proof. Let α^* be the solution to the optimization problem (27). By (C1) and (25), $(\vartheta(\alpha^*), \dot{\vartheta}(\alpha^*)) \in \mathbf{Z}_{\alpha^*}$. Moreover, by (23) (specifically, the fact that $h_R(\vartheta(\alpha^*)) = 0$) and (C3), it follows that $(\vartheta(\alpha^*), \dot{\vartheta}(\alpha^*)) \in S_R$. Therefore, $(\vartheta(\alpha^*), \dot{\vartheta}(\alpha^*)) \in S_R \cap \mathbf{Z}_{\alpha^*}$. Now, $\mathbf{Z}_{\alpha^*}$ and S_R intersect transversally since

$$L_{f_R} h_R(\vartheta(\alpha^*), \dot{\vartheta}(\alpha^*)) = dh_R(\vartheta(\alpha^*))\dot{\vartheta}(\alpha^*) < 0$$

by (C3). Since $\mathbf{Z}_{\alpha^*}$ is a 1-dimensional submanifold of X_R, it follows that $S_R \cap \mathbf{Z}_{\alpha^*}$ is a unique point. Therefore, $(\vartheta(\alpha^*), \dot{\vartheta}(\alpha^*)) = S_R \cap \mathbf{Z}_{\alpha^*}$.

To show that $\Delta_R(S_R \cap \mathbf{Z}_{\alpha^*}) \subset \mathbf{PZ}_{\alpha^*}$ we need only show that $\Delta_R(\vartheta(\alpha^*), \dot{\vartheta}(\alpha^*)) \in \mathbf{PZ}_{\alpha^*}$. Since

$$\Delta_R(\vartheta(\alpha^*), \dot{\vartheta}(\alpha^*)) = \begin{bmatrix} \mathscr{R}\vartheta(\alpha^*) \\ \mathscr{R}\mathscr{P}(\vartheta(\alpha^*))\dot{\vartheta}(\alpha^*) \end{bmatrix}$$

from (5), the requirement that $\Delta_R(\vartheta(\alpha^*), \dot{\vartheta}(\alpha^*)) \in \mathbf{PZ}_{\alpha^*}$ is equivalent to the following conditions being satisfied:

$$y_2(\mathscr{R}\vartheta(\alpha^*)) = 0, \tag{28}$$

$$L_{f_R} y_2(\mathscr{R}\vartheta(\alpha^*), \mathscr{R}\mathscr{P}(\vartheta(\alpha^*))\dot{\vartheta}(\alpha^*)) = 0. \tag{29}$$

By the definition of $\vartheta(\alpha^*)$, and specifically (23), (28) is satisfied. Moreover,

$$L_{f_R} y_2 \mathscr{R}\vartheta(\alpha^*), \mathscr{R}\mathscr{P}(\vartheta(\alpha^*))\dot{\vartheta}(\alpha^*) = dy_2(\mathscr{R}\vartheta(\alpha^*))\mathscr{R}\mathscr{P}(\vartheta(\alpha^*))\dot{\vartheta}(\alpha^*)$$

Therefore, (29) is satisfied as a result of (C2). Thus we have established that $\Delta_R(S_R \cap \mathbf{Z}_{\alpha^*}) \subset \mathbf{PZ}_{\alpha^*}$. $\square$

Remark on Theorem 1. Note that if the goal was to obtain full hybrid zero dynamics: $\Delta_R(S_R \cap \mathbf{Z}_\alpha) \subset \mathbf{Z}_\alpha$, then the theorem would be exactly as stated, except condition (C2) would become:

$$Y(\mathscr{R}\vartheta(\alpha))\mathscr{R}\mathscr{P}(\mathscr{R}\vartheta(\alpha))\dot{\vartheta}(\alpha) = \begin{bmatrix} v_{\text{hip}} \\ \mathbf{0} \end{bmatrix}. \tag{C2'}$$

We also numerically solved the optimization in this case, but while we were able to find a solution, we were unable to accurately fit the human data; specifically, we could fit all the human outputs well except the stance knee (the pattern repeated for PHZD, but to a much smaller degree). We argue that this is due to differences in the model of the robot and the human; thus, constraining the robot to evolve on the 1-dimensional surface, $\mathbf{Z}_\alpha$, is too restrictive to result in "good" robotic walking.

PHZD Optimization Results. By solving the optimization problem in Theorem 1, we are able to determine parameters α^* that automatically guarantee PHZD for the hybrid system $\mathscr{H}_R^{(\alpha^*,\varepsilon)}$ modeling the bipedal robot. In addition to the constraints in Theorem 1, when running this optimization we added the constraint that $\tau(\vartheta(\alpha)) \leq t^H[K]$, with $t^H[K]$ the last time for which there is data for the human, i.e., the duration of one step; this ensures that canonical human walking functions can be compared to the human output data over the entire step. It is important to note that this optimization does not require us to solve any of the dynamics for $\mathscr{H}_R^{(\alpha,\varepsilon)}$ due to the independence of the conditions (C1)-(C3) on state, i.e., they can be computed

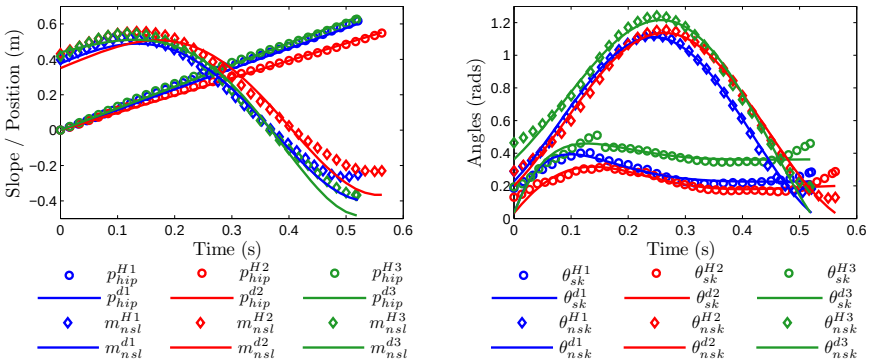

(a) Hip Position and Non-Stance Leg Slope (b) Stance and Non-stance Knee Angle

Fig. 5: The human output data and the canonical walking function fits for each subject obtained by solving the optimization problem in Theorem 1.

in closed form from the model of the robot. Therefore, the optimization in Theorem 1 can be numerically solved in a matter of seconds[2].

The results of this optimization can be seen in Fig. 5, with the specific parameter values given in Table 2. In particular, note that with the exception of the stance knee θ_{sk}, all of the correlations are between 0.9850 and 0.9995, indicating that an exceptionally close fit to the human data is possible, even while simultaneously satisfying the PHZD conditions. The stance knee is an exception here; while the fits are still good, they have slightly lower correlations. This is probably due to the fact that the stance knee bears the weight of the robot, and hence is more sensitive to differences between the model of the robot and the human. That being said, it is remarkable how close the canonical human functions can be fit to the human data since the constraints depend on the model of the robot, which obviously has very different dynamics than that of the human.

6 Automatically Generating Stable Robotic Walking

This section demonstrates through simulation that the parameters α^* solving the optimization problem in Theorem 1 automatically produce an exponentially stable periodic orbit, i.e., a stable walking gait, for which $(\vartheta(\alpha^*), \dot{\vartheta}(\alpha^*))$ is the fixed point. That is, using the human data, we are able to automatically generate parameters for the controller (17) that result in stable walking for which the partial zero dynamics are hybrid invariant. We also demonstrate the extensibility of the canonical human walking functions by showing that they also can be used to obtain stable

[2] Note that the optimization problem is prone to local minima, so it is likely that there are better fits to the human data than reported.

Table 2: Parameter values of the canonical walking functions for the 3 subjects, obtained by solving the optimization problem in Theorem 1, together with the cost and correlations of the fits.

$y_{H,1} = vt$ $y_{H,2} = e^{-\alpha_4 t}(\alpha_1 \cos(\alpha_2 t) + \alpha_3 \sin(\alpha_2 t)) + \alpha_5$									
S	Fun.	v	α_1	α_2	α_3	α_4	α_5	Cost	Cor.
1	p_{hip}	1.1534	*	*	*	*	*	0.2152	0.9995
	m_{nsl}	*	0.1407	7.7813	0.1332	-2.2899	0.2359		0.9940
	θ_{sk}	*	-0.1942	9.1241	0.8089	11.490	0.2290		0.9185
	θ_{nsk}	*	-0.3248	9.2836	0.4103	-0.2790	0.5517		0.9960
2	p_{hip}	0.9812	*	*	*	*	*	0.3055	0.9992
	m_{nsl}	*	0.0731	8.1450	0.1355	-2.6624	0.2774		0.9850
	θ_{sk}	*	-0.1677	11.852	0.2684	6.3379	0.2010		0.9074
	θ_{nsk}	*	-0.3667	-8.8272	-0.4053	-0.1707	0.5662		0.9959
3	p_{hip}	1.2287	*	*	*	*	*	0.2949	0.9990
	m_{nsl}	*	0.0876	7.9627	0.0552	-4.2023	0.3517		0.9944
	θ_{sk}	*	-0.3283	10.279	0.5051	11.273	0.3638		0.8877
	θ_{nsk}	*	-0.2432	8.6235	0.4105	-0.9881	0.6053		0.9947

robotic walking in the case of underactuation at the stance ankle. Thus, the ideas presented here are not fundamentally limited to fully actuated systems (unlike other popular methods for producing robotic walking such as controlled symmetries [27] and geometric reduction [6], which build upon principles of passive walking [18] and require full actuation to modify the Lagrangian of the robot).

Walking Gaits from the PHZD Optimization. Before discussing the simulation results of this paper, we justify why robotic walking automatically results from solving the PHZD Optimization in Theorem 1. In particular, let α^* be the solution to the optimization problem (27) in Theorem 1. Then the claim is that there exists an $\overline{\varepsilon} > 0$ such that for all $\varepsilon > \overline{\varepsilon}$ the hybrid system $\mathscr{H}_R^{(\alpha^*,\varepsilon)}$ has a locally exponentially stable periodic orbit $\mathscr{O}_{\alpha^*} \subset \mathbf{PZ}_{\alpha^*}$. Moreover, $(\vartheta(\alpha^*), \dot{\vartheta}(\alpha^*)) \in S_R \cap \mathbf{Z}_{\alpha^*}$ is "sufficiently" close to the fixed point of this periodic orbit and $\tau(\vartheta(\alpha^*)) > 0$ is "sufficiently" close to its period. Informally speaking, this follows from the fact that for *full* hybrid zero dynamics, i.e., $\Delta_R(S_R \cap \mathbf{Z}_\alpha) \subset \mathbf{Z}_\alpha$, these statements can be proven by using the low dimensional stability test of [33] (with the restricted Poincaré map being trivial), coupled with the fact that points in $\mathbf{PZ}_{\alpha^*}$ will converge exponentially fast to the surface $\mathbf{Z}_{\alpha^*}$. We justify these statements further through the use of simulation results.

Robotic Walking with PHZD. To demonstrate how we automatically generate robotic walking from the human data, we do so for each of the subjects considered in this paper. In particular, consider the bipedal robot in Fig. 1 with the mass and length parameters specific to each of the three subjects according to Fig. 2, from which we construct a hybrid system model, $\mathscr{H}_{R,i}^{(\alpha,\varepsilon)}$ with $i = 1,2,3$, for each according to (19) utilizing the human-inspired controllers. Applying Theorem 1, we automatically obtain the set of parameters α_i^* such that $\mathscr{H}_{R,i}^{(\alpha_i^*,\varepsilon)}$ is guaranteed to

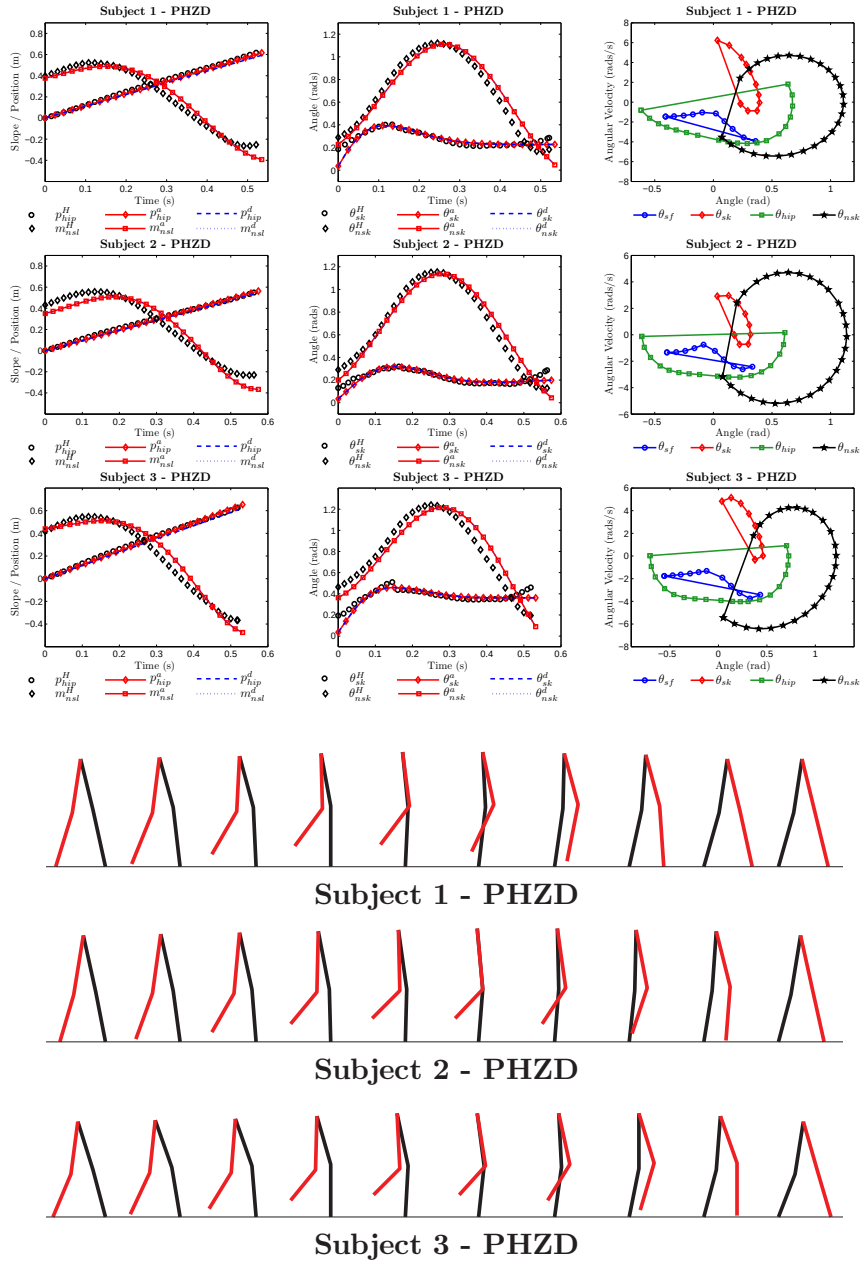

Fig. 6: The human data compared to the actual and desired canonical human walking functions for the 3 subjects over one step with the parameters that guarantee PHZD as determined by Theorem 1 (left and middle column), along with the corresponding periodic orbits (right column) and tiles of the walking for each subject (bottom).

(a) Eigenvalues

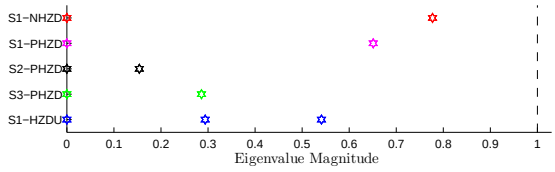

(b) Fixed Points

Sub.	S_1	S_1	S_2	S_3	S_1
Type	NHZD	PHZD	PHZD	PHZD	HZDU
θ_{sf}	-0.475	-0.469	-0.444	-0.599	-0.386
θ_{sk}	0.255	0.227	0.199	0.362	0.119
θ_{hip}	-0.681	-0.637	-0.610	-0.703	-0.747
θ_{nsk}	0.187	0.035	0.033	0.036	0.545
$\dot{\theta}_{sf}$	-1.703	-1.492	-1.337	-1.788	-0.620
$\dot{\theta}_{sk}$	0.331	0.020	0.114	0.020	-1.853
$\dot{\theta}_{hip}$	-0.748	-0.472	-0.220	0.462	5.943
$\dot{\theta}_{nsk}$	-2.764	-3.065	-2.556	-5.364	-8.404

Fig. 7: The magnitude of the eigenvalues (a) associated with the periodic orbits with fixed points (b) for Subject 1 in the non-HZD case, Subject 1-3 in the case of PHZD, and Subject 1 in the underactuated HZD case.

have partial hybrid zero dynamics. Moreover, the explicit functions used to compute this vector of parameters automatically produces the point $(\vartheta(\alpha_i^*), \dot{\vartheta}(\alpha_i^*))$ that, as will be seen, is a fixed point to an exponentially stable periodic orbit. Thus, for each of the subjects, using only their physical parameters and walking data, we automatically and provably obtain stable walking gaits.

The walking gaits that are obtained for each of the subjects through the aforementioned methods can be seen in Fig. 6, where the walking is simulated over the course of one step with $\varepsilon = 20$. The specific periodic orbits can be seen in the right column of that figure with the fixed points given in Fig. 7. Moreover, stability of the walking is verified by computing the eigenvalues of the Poincaré map; these values can also be found in Fig. 7. Note that, unlike the robotic walking in the case where hybrid zero dynamics were not enforced (as discussed in Sect. 4), the velocities of the robot are much more reasonable (with a maximum value of approximately $6\frac{rad}{s}$ for Subject 1 as opposed to exceeding $12\frac{rad}{s}$ as in the non-HZD case). This is a very interesting byproduct of the fact that the optimization appears to automatically converge to a fixed point $(\vartheta(\alpha_i^*), \dot{\vartheta}(\alpha_i^*))$ in which the non-stance leg is essentially locked at foot impact $(\vartheta(\alpha_i^*)_{nsk} \approx 0)$, and thus the shocks due to impact are naturally absorbed by the mechanical components of the system rather than having to be compensated for through actuation. This can be visually verified in the tiles of the walking gait in Fig. 6 and perhaps, even better, in the movies of the robotic walking obtained (see [1]).

There are some noteworthy aspects of the relationships between the robotic walking obtained and the human data from which it was derived. In particular, as can be seen in the left and middle columns of Fig. 6, the actual and desired relative degree 2 outputs agree for all time; thus partial hybrid zero dynamics has been verified through simulation, and the canonical walking function fits produced by Theorem 1 (as seen in Fig. 5) are the actual outputs of the robot. In addition, while the relative degree 1 output is not invariant through impact, its change is so small that it cannot be seen in the plots. It is interesting to note that the largest deviation from the human outputs is at the beginning and at the end of the step. This makes intuitive sense: the robot, unlike the human, does not have feet, so the largest differences between the

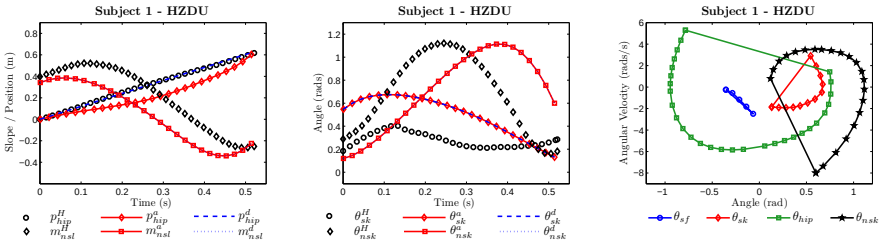

(a) p_{hip} and m_{nsl} (b) θ_{sk} and θ_{nsk} (c) Periodic Orbit

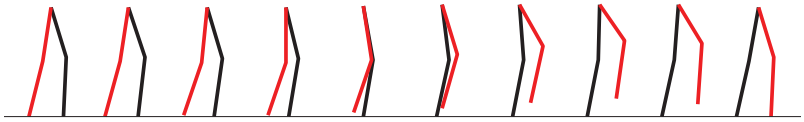

(d) Walking Tiles

Fig. 8: Walking obtained for Subject 1 with hybrid zero dynamics and underactuation at the stance ankle, with (a)-(b) the actual and desired outputs vs. the human output data over one step, (c) the periodic orbit and (d) the tiles (or snapshots) of the walking gait.

two models occur when the feet play a more active role which, in the case of this data, is at the beginning and end of the step (see [25] for a formal justification of this statement). Moreover, the robot and the human react much differently to the impact with the ground, which is again due to the presence of feet and the fact that the robot is rigid while the human is compliant. Thus, the deviations pre- and post-impact are largest due to these differences, and also due to the fact that in the robot we enforce partial hybrid zero dynamics. All that being said, the agreement between the outputs of the robot and the human output data is remarkable. It is, therefore, reasonable to conclude that we have achieved "human-like" robotic walking. Readers are invited to draw their own conclusions by watching the movie of the robotic walking achieved by referring to [1] and related videos at [3].

Underactuated Human-Inspired HZD. To demonstrate the extensability of the methods introduced in this paper, we apply them in the case when the robot being considered is underactuated; specifically, the stance ankle cannot be controlled. This is more "realistic" for the robot being considered due to the fact that it has point feet. As will be seen, this restriction on the actuation of the robot will result in less "human-like" walking, which naturally follows from the fact that humans actively use their stance ankle when walking.

For the sake of brevity, we consider the hybrid system associated with Subject 1, $\mathscr{H}_R^{(\alpha,\varepsilon)}$, where in this case we remove the actuation at the ankle. The control law for this system therefore becomes the control law in (17) with the top row removed

and with decoupling matrix A as in (18) again with the top row removed. Moreover, in this case $\mathbf{Z}_\alpha = \mathbf{P}\mathbf{Z}_\alpha$, i.e., the full and partial hybrid zero dynamics are just the classical hybrid zero dynamics as considered in [33]. Therefore, the optimization problem in Theorem 1 ensures hybrid zero dynamics *if* $(\vartheta(\alpha), \dot{\vartheta}(\alpha))$ is an initial condition to a stable periodic orbit. Note that, unlike the case with full actuation, it is necessary to simulate the system to ensure that this is the case; as a result, the optimization is dramatically slower (producing a solution in approximately 12 minutes as opposed to 10 seconds).

The end result of solving the optimization in Theorem 1 is a stable periodic orbit with hybrid zero dynamics. The walking that is obtained can be seen in Fig. 8, where the outputs of the robot and the human are compared, the periodic orbit is shown, along with tiles of the walking gait. It is interesting to note that the behavior of the walking in the case of underactuated HZD is substantially different than the walking for fully-actuated PHZD. In particular, due to the lack of actuation at the ankle, the robot swings its leg dramatically forward in order to push the center of mass in front of the stance ankle. What is remarkable is that this change in behavior was not hard coded, but rather naturally resulted from the optimization. This provides further evidence for the fact that the human walking functions are, in fact, canonical since they can be used to achieve a variety of walking behaviors.

7 Conclusions and Future Challenges

This paper presents the first steps toward automatically generating robotic walking from human data. To achieve this goal, the first half of the paper introduces three essential constructions: (1) define human outputs that appear characteristic of walking, (2) determine canonical walking functions describing these outputs, and (3) use these outputs and walking functions, in the form of human-inspired outputs for a bipedal robot, to design a human-inspired controller. We obtain parameters for this control law through an optimization problem that guarantees PHZD and that explicitly produces a fixed point to an exponentially stable periodic orbit contained in the zero dynamics surface. A 2D bipedal robot with knees is considered and these results are applied to experimental walking data for a collection of subjects, allowing us to automatically generate stable robotic walking that is as close to the human data as possible, i.e., walking that is as "human-like" as possible.

While the results of this paper are limited to a simple bipedal robot, human-inspired controllers have been used to achieve robotic walking for 2D bipeds with knees, feet and a torso [25] and 3D bipeds with knees and a torso [24] (illustrated in Fig. 9). Yet formal results ensuring hybrid zero dynamics and proving the existence of a stable periodic orbit have yet to be established. The difficulty in extending the results of this paper comes from the discrete phases of walking present in more anthropomorphic bipedal robots due to the behavior of the feet [7]. On each domain human outputs must be defined and canonical walking functions determined in such a way that, using only the human data, parameters for the corresponding

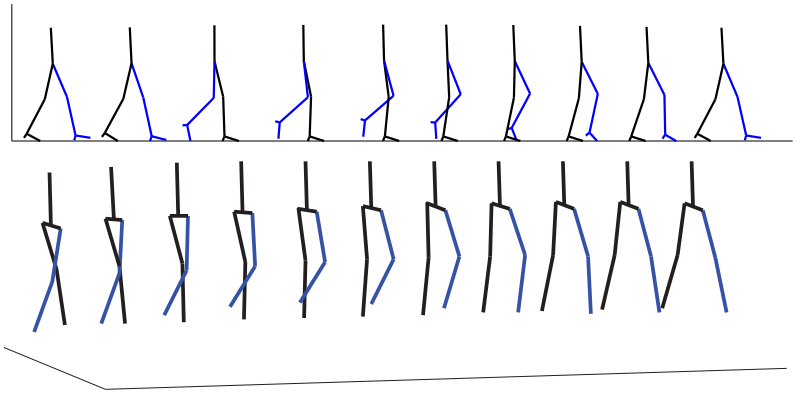

Fig. 9: Tiles of the walking gaits obtained through the use of human-inspired outputs for a 2D robot with feet, knees and a torso (top) and a 3D robot with knees and a torso (bottom) utilizing the data for Subject 1.

human-inspired controllers can be determined so as to guarantee (partial) hybrid zero dynamics throughout the entire step. This points toward a collection of challenging problems, the solutions for which could allow for the automatic generation of human-like robotic walking from human data.

To provide concrete objectives related to the overarching goal of obtaining truly human-like walking for anthropomorphic bipedal robots, as motivated by the ideas related to this paper, we lay out a serious of "challenge problems" for human-inspired bipedal robotic walking:

Problem 1: Obtain *human-inspired hybrid system models* of anthropomorphic bipedal robots.

Problem 2: Determine *outputs* of the human to consider and associated *human walking functions* that are *canonical*.

Problem 3: Use Problem 2 to design *human-inspired controllers* and obtain formal conditions that guarantee hybrid zero dynamics (either full or partial).

Problem 4: Determine the parameters of these controllers *automatically from human data* using no a priori knowledge about the data.

Problem 5: Provably and automatically *produce stable periodic orbits*, i.e., stable walking gaits, that are as "human-like" as possible.

Importantly, the solutions of these problems must go beyond the task of achieving flat-ground straight-line walking, but rather should be automatically extensible to a wide variety of walking behaviors, or *motion primitives*, e.g., walking up and down slopes, stair-climbing, turning left and right, walking on uneven terrain. It is therefore necessary to determine methods for transition between walking motion primitives, formally encoded as solutions to Problems 1-5, so that stability is maintained. Finally, in order to truly demonstrate the validity of specific solutions to the

challenge problems, it is necessary to ultimately realize them on physical bipedal robots.

The solutions to these challenge problems would have far-reaching ramifications for our understanding of both robotic and human walking. They would result in bipedal robots able to produce the variety of walking behaviors that allow humans to navigate diverse terrain and environments with ease, resulting in important applications to areas like space exploration. In addition, they would have potentially revolutionary applications to all areas in which humans and robots interact to achieve locomotion—from rehabilitation, prosthetic and robotic assistive devices able to supplement impaired walking to aiding the walking of healthy humans through exoskeleton design.

Acknowledgements. I would like to thank Matthew Powell for his contribution in generating figures and parts of the code used to display the results of this paper, Ryan Sinnet for his contributions to human-inspired control that led to this work, and Ram Vasudevan for many conversations on the role of optimization in automatically generating robotic walking from human data and for helping to run the experiments discussed in this paper. I am also grateful Jessy Grizzle for the many insightful discussions on bipedal walking over the years, and Ruzena Bajcsy for introducing me to the world of experimentation.

References

1. Movie of of the robotic walking obtained via human-inspired hybrid zero dynamics. `http://www.youtube.com/watch?v=72hSW44qMgw`
2. Website for data set and related papers. `http://www.eecs.berkeley.edu/~ramv/HybridWalker`
3. YouTube page for AMBER lab. `http://www.youtube.com/user/ProfAmes`
4. Ambrose, R., Aldridge, H., Askew, R., Burridge, R., Bluethmann, W., Diftler, M., Lovchik, C., Magruder, D., Rehnmark, F.: Robonaut: NASA's space humanoid. IEEE Intelligent Systems and their Applications **15**(4), 57 –63 (2000)
5. Ames, A.D., Gregg, R., Wendel, E., Sastry, S.: On the geometric reduction of controlled three-dimensional bipedal robotic walkers. In: Lagrangian and Hamiltonian Methods for Nonlinear Control 2006, *Lecture Notes in Control and Information Sciences*, vol. 366, pp. 183–196. Springer (2007)
6. Ames, A.D., Sinnet, R.W., Wendel, E.D.B.: Three-dimensional kneed bipedal walking: A hybrid geometric approach. In: R. Majumdar, P. Tabuada (eds.) 12th ACM Intl. Conf. on Hybrid Systems: Computation and Control, Lecture Notes in Computer Science—HSCC 2009, vol. 5469, pp. 16–30. San Francisco (2009)
7. Ames, A.D., Vasudevan, R., Bajcsy, R.: Human-data based cost of bipedal robotic walking. In: Hybrid Systems: Computation and Control. Chicago, IL (2011)
8. Au, S.K., Dilworth, P., Herr, H.: An ankle-foot emulation system for the study of human walking biomechanics. In: IEEE Intl. Conf. Robotics and Automation, pp. 2939–2945. Orlando (2006)
9. Braun, D.J., Goldfarb, M.: A control approach for actuated dynamic walking in bipedal robots. IEEE TRO **25**(6), 1292–1303 (2009)
10. Chevallereau, C., Bessonnet, G., Abba, G., Aoustin, Y.: Bipedal Robots: Modeling, Design and Walking Synthesis. Wiley-ISTE, New York (2009)

11. Chevallereau, C., Formal'sky, A., Djoudi, D.: Tracking a joint path for the walk of an underactuated biped. Robotica **22**(1), 15–28 (2004)
12. Childs, D.W.: Dynamics in Engineering Practice, 10 edn. CRC Press (2010)
13. Grizzle, J.W., Abba, G., Plestan, F.: Asymptotically stable walking for biped robots: Analysis via systems with impulse effects. IEEE TAC **46**(1), 51–64 (2001)
14. Grizzle, J.W., Chevallereau, C., Ames, A.D., Sinnet, R.W.: 3D bipedal robotic walking: models, feedback control, and open problems. In: IFAC Symposium on Nonlinear Control Systems. Bologna (2010)
15. Heller, M.O., Bergmann, G., Deuretzbacher, G., Dürselen, L., Pohl, M., Claes, L., Haas, N.P., Duda, G.N.: Musculo-skeletal loading conditions at the hip during walking and stair climbing. J. of Biomechanics **34**(1), 883–893 (2001)
16. Hürmüzlü, Y., Marghitu, D.B.: Rigid body collisions of planar kinematic chains with multiple contact points. Intl. J. of Robotics Research **13**(1), 82–92 (1994)
17. Kuo, A.D.: Energetics of actively powered locomotion using the simplest walking model. Journal of Biomechanical Engineering **124**, 113–120 (2002)
18. McGeer, T.: Passive dynamic walking. Intl. J. of Robotics Research **9**(2), 62–82 (1990)
19. Morris, B., Grizzle, J.: A restricted Poincaré map for determining exponentially stable periodic orbits in systems with impulse effects: Application to bipedal robots. In: IEEE Conf. on Decision and Control. Seville, Spain (2005)
20. Murray, R.M., Li, Z., Sastry, S.S.: A Mathematical Introduction to Robotic Manipulation. CRC Press, Boca Raton (1994)
21. Sastry, S.S.: Nonlinear Systems: Analysis, Stability and Control. Springer, New York (1999)
22. Sauer, P., Kozlowski, K., Morita, Y., Ukai, H.: Ankle robot for people with drop foot—case study. In: K. Kozlowski (ed.) Robot Motion and Control 2009, *Lecture Notes in Control and Information Sciences*, vol. 396, pp. 443–452. Springer (2009)
23. Schaub, T., Scheint, M., Sobotka, M., Seiberl, W., Buss, M.: Effects of compliant ankles on bipedal locomotion. In: EEE/RSJ International Conference on Intelligent Robots and Systems. 2009
24. Sinnet, R., Powell, M., Jiang, S., Ames, A.D.: Compass gait revisited: A human data perspective with extensions to three dimensions. Submitted for publication, available upon request
25. Sinnet, R., Powell, M., Shah, R., Ames, A.D.: A human-inspired hybrid control approach to bipedal robotic walking. In: 18th IFAC World Congress. Milano, Italy (2011)
26. Sinnet, R.W., Ames, A.D.: 2D bipedal walking with knees and feet: A hybrid control approach. In: 48th IEEE Conference on Decision and Control. Shanghai, P.R. China (2009)
27. Spong, M.W., Bullo, F.: Controlled symmetries and passive walking. IEEE TAC **50**(7), 1025–1031 (2005)
28. Srinivasan, S., Raptis, I.A., Westervelt, E.R.: Low-dimensional sagittal plane model of normal human walking. ASME J. of Biomechanical Eng. **130**(5) (2008)
29. Srinivasan, S., Westervelt, E., Hansen, A.: A low-dimensional sagittal-plane forward-dynamic model for asymmetric gait and its application to study the gait of transtibial prosthesis users. ASME J. of Biomechanical Eng. **131** (2009)
30. Vasudevan, R., Ames, A.D., Bajcsy, R.: Using persistent homology to determine a human-data based cost for bipedal walking. In: 18th IFAC World Congress. Milano, Italy (2011)
31. Vukobratović, M., Borovac, B., Surla, D., Stokic, D.: Biped Locomotion. Springer-Verlag, Berlin (1990)
32. Wendel, E., Ames, A.D.: Rank properties of Poincaré maps for hybrid systems with applications to bipedal walking. In: Hybrid Systems: Computation and Control. Stockholm, Sweden (2010)
33. Westervelt, E.R., Grizzle, J.W., Chevallereau, C., Choi, J.H., Morris, B.: Feedback Control of Dynamic Bipedal Robot Locomotion. CRC Press, Boca Raton (2007)
34. Westervelt, E.R., Grizzle, J.W., Koditschek, D.E.: Hybrid zero dynamics of planar biped walkers. IEEE TAC **48**(1), 42–56 (2003)
35. Winter, D.A.: Biomechanics and Motor Control of Human Movement, 2 edn. Wiley-Interscience, New York (1990)
36. Zatsiorsky, V.M.: Kinematics of Human Motion, 1 edn. Human Kinetics (1997)